

Characterizing adaptive behavior of the wrist during lateral force perturbations

Andria J. Farrens, *Student Member, IEEE* and Fabrizio Sergi, *Member, IEEE*

Abstract—Combining functional magnetic resonance imaging (fMRI) with models of neuromotor adaptation is useful for identifying the function of different neuromotor control centers in the brain. Current models of neuromotor adaptation to force perturbations have been studied primarily in whole-arm reaching tasks that are ill-suited for MRI. We have previously developed the MR-SoftWrist, an fMRI-compatible wrist robot, to study motor control during wrist adaptation. Because the wrist joint has intrinsic dynamics dominated by stiffness, it is unclear if these models will apply to the wrist.

Here, we characterize adaptation of the wrist to lateral forces to determine if established adaptation models are valid for wrist pointing. We recruited thirteen subjects to perform our task using the MR-SoftWrist. Our task included a clockwise (CW) – counterclockwise (CC) – error clamp schedule and an alternating CW-CC force field schedule. To determine applicability of previous models, we fit three candidate models — a single-state, two-state, and context dependent multi-state model — to behavioral data.

Our results indicate that features of sensorimotor adaptation reported in the literature are present in the wrist, including spontaneous recovery, and anterograde and retrograde interference between the learning of two oppositely directed force fields. A two-state model best fit our behavioral data. Under this model, adaptation was dominated by a fast learning state with minor engagement of a slow learning state. Finally, all adaptation models tested showed a consistent over-estimation of performance error, suggesting that the control of the wrist relies not only on internal models but likely other mechanisms, like impedance control, to reject perturbations.

I. INTRODUCTION

Robot-mediated neurorehabilitation (RMN) uses robots as tools to retrain upper extremity motor control in chronic stroke patients. Currently, patient outcomes following RMN are no better than those seen in traditional therapy [1]. To advance RMN, the neurological basis for motor learning using such robotic devices needs to be better understood.

Whole-brain techniques such as functional magnetic resonance imaging (fMRI) are well suited to study the distributed brain regions involved in motor function and learning [2], [3]. Our group has developed the MR-SoftWrist, an fMRI-compatible 3 degree of freedom (DOF) wrist robot, to study neuromotor control in robot-assisted sensorimotor tasks involving the wrist joint via fMRI [4], [5]. To identify brain regions responsible for specific neuromotor control mechanisms, we plan to combine models of sensorimotor adaptation with fMRI measures of neural activity.

Previous studies show that the brain controls movement in a feed-forward manner based on an internal model of

the required task dynamics. When movements based on this model result in movement error, the error is used to update the internal model to generate corrected motor commands for the next movement [2], [3]. Numerous computational models have been proposed to describe how the brain updates and selects these internal models, including single-state, two-state, and multi-state models [6], [7]. These models have been proposed to describe behavior in upper extremity tasks involving the shoulder and elbow under force fields [6], [8]–[10], and in visuomotor distortion tasks involving distal joints such as the wrist and fingers [7], [11], [12]. In these studies, the quantitative features of the modeled behavior varied with the dynamics of the task performed. Moreover, as the wrist has intrinsic dynamics dominated by stiffness, control of wrist may rely on different mechanisms than control of the shoulder and elbow [13], [14]. As such, we cannot assume that previously proposed models will apply to dynamic wrist pointing tasks.

To use models of adaptation to identify neural mechanisms of motor control, we first need to determine if current models of neuromotor control apply to the wrist. The validity of different models can be tested using specific task sequences capable of eliciting distinguishable behavior. An A-B-EC task design, in which subjects adapt to an initial perturbation (A), followed by brief exposure to an oppositely directed perturbation (B), before having their errors clamped to zero (EC), can elicit spontaneous recovery, a rebound of behavior that reflects adaptation to the first perturbation (A) [6], [9]. Importantly, this behavior is only predicted by models with more than one state that can account for savings of the initial adaptation that drive the apparent “spontaneous recovery”. An alternating A-B task design, in which two opposite perturbations are presented in an alternating schedule, can elicit interference or dual adaptation behaviors [7], [10], [15]. Interference can be described by a two-state model, with one fast and one slow state, while dual adaptation is best described by a multi-state model with a single fast state and multiple context dependent slow states.

To our knowledge, we are the first group to study adaptation of the wrist in two DOFs to lateral force fields [3]. To characterize the adaptive behavior of the wrist, we recruited subjects to perform an A-B-EC task followed by an alternating A-B task. We fit a single-state, two-state and multi-state model to measured behavior to determine which model, if any, best characterize adaptation of the wrist to lateral force fields. The A-B-EC task schedule was used to test for spontaneous recovery, and the A-B task was used to test for the presence of interference and/or dual adaptation.

FS (corresponding author - fabs@udel.edu), and AJF are with the Human Robotics Laboratory, Department of Biomedical Engineering, University of Delaware, Newark DE, 19713 USA.

II. MATERIALS AND METHODS

A. Subjects

Thirteen subjects (8 male, aged 22-29) gave their informed consent to participate in our study (IRBNet ID:906215-7). Subjects performed the task with their dominant hand (3 left, 10 right). We excluded one subject (M, left) for performing >50% of trials too slowly (>500 ms), and one (M, right) due to hardware failure.

B. MR-SoftWrist

Our wrist pointing task was performed using the MR-SoftWrist (Fig. 1, top). Subjects held the handle of the MR-SoftWrist to move a cursor displayed on a monitor. Flexion-extension (FE) of the wrist moved the cursor horizontally, while radial-ulnar deviation (RUD) moved the cursor vertically. Pronation-supination was prevented by a forearm support. Subjects were cued to make alternating FE rotations to move a cursor in a straight line to one of two targets located at ($\pm 10, 0$) degrees in FE, RUD respectively. Trial onset was cued by a change in target color from black to blue. At trial completion the reached target provided timing feedback by turning red if movement duration was > 450 ms or green if it was < 250 ms. Otherwise it remained black.

The robot acted in three operational conditions during task performance; i) A no force condition, in which the robot acts transparently to measure baseline performance with minimal interaction forces (Fig.1, bottom left). ii) A velocity-dependent force field condition, in which the robot applies forces lateral to the direction of movement [2], [16].

$$\begin{bmatrix} \tau_{FE} \\ \tau_{RUD} \end{bmatrix} = \alpha \begin{bmatrix} 0 & 1 \\ -1 & 0 \end{bmatrix} \cdot \begin{bmatrix} \dot{\theta}_{FE} \\ \dot{\theta}_{RUD} \end{bmatrix} \quad (1)$$

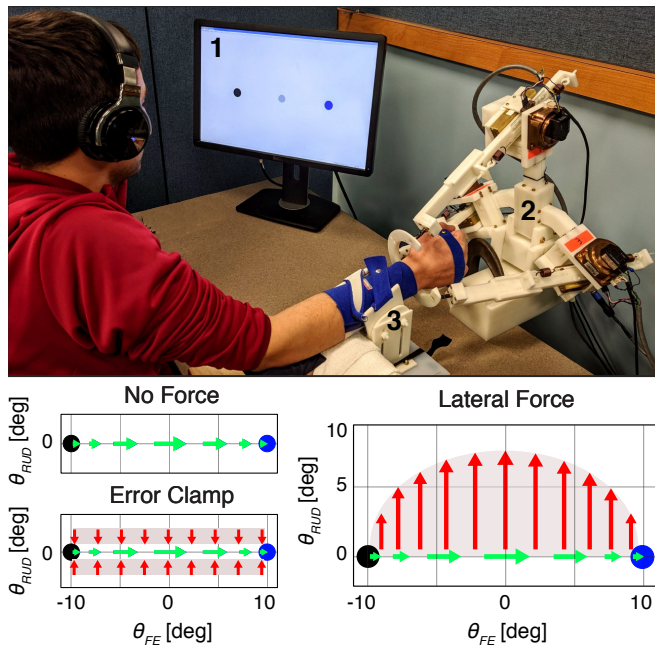


Fig. 1. Top: MR-SoftWrist during task performance. [1] Visual display [2] MR-SoftWrist [3] Forearm support. Bottom: Task force conditions

In eq. 1, $\dot{\theta}$ is the measured angular velocity of the wrist (deg/s), while τ corresponds to the robot applied torques about the wrist joint, shown in Fig.1, bottom right. Clockwise and counter-clockwise force fields were achieved with $\alpha = \pm 250$ mNms/deg, respectively. Finally, iii) An error-clamp condition, in which the robot produces a force channel that clamps trajectory error to zero, was used to measure subjects lateral force profiles that reflect their expectation of required task dynamics. Due to inherent compliance of our robot the effective error clamp channel width was ± 0.5 degrees.

C. Task Design

To characterize adaptive behavior, an adaptation task needs to 1) guarantee identifiability of all parameters in a given model; and 2) be designed so that expected behavior from each candidate model is maximally different to enable identification of the most plausible model from the measured data.

To achieve both goals, we used an A-B-EC task and an alternating A-B force field task. The A-B-EC task can elicit spontaneous recovery, behavior that both the two-state and multi-state model, but not the single-state model, can adequately describe. The alternating A-B task can elicit either dual adaptation behavior where subjects adapt to both force fields simultaneously, or interference where learning of one force field interferes with learning of the other. Dual adaptation is best described by a multi-state model with context-dependent slow states, while interference between the two force fields is better predicted by a two-state model.

Our task is shown in Fig. 2. In part 1 subjects performed wrist pointing in a no force condition; in part 2 subjects performed the A-B-EC task; in part 3 they performed the alternating A-B task. EC trials were dispersed throughout with a 1/8 frequency in a pseudorandom manner that ensured trials were > 4 and < 12 trials apart, except for the N_3 and N_4 blocks of the A-B-EC task [6]. No visual or auditory cue was given for subjects to distinguish between force field type. Instead, contextual switching was assumed to occur after exposure to error on the first trial of a any condition [7]. A break was given between parts 1, 2, and 3 to reduce fatigue, during which subjects remained in the forearm support and

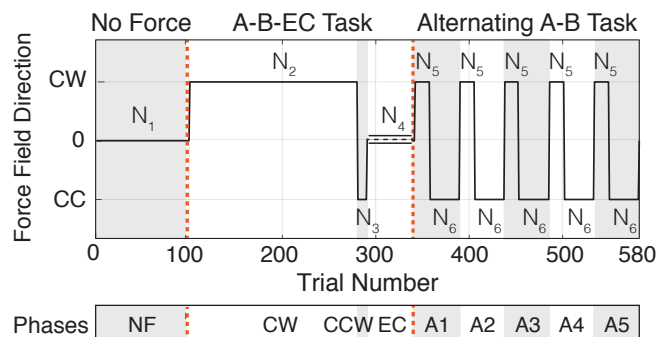


Fig. 2. Task Design. Part 1, 2 and 3 are divided by red dashes. Here, $N_1 = 100$, $N_2 = 180$, $N_3 = 10$, $N_4 = 50$, $N_5 = 16$ and $N_6 = 32$ trials. N_3 had no EC trials while N_4 consisted entirely of EC trials. Bottom block shows experimental phases used for statistical analyses.

did not change physical orientation. To reduce environmental distractions, subjects wore noise canceling headphones that played white noise during each task.

D. Models of Motor Adaptation

Motor adaptation, an error driven learning process that enables adjustment of movement to new demands, is an important mechanism used by the central nervous system (CNS) to control movement [2]. The CNS controls movement, in part, in a feed-forward manner based on an internal model of expected limb and environmental dynamics. The CNS updates its internal model in response to changes in task dynamics through error feedback; movement based on the internal model that results in error is used to re-calibrate the internal model and change subsequent motor output.

Adaptation to force perturbations has been extensively studied during reaching using lateral force fields, and in 1 DOF tasks in the wrist using assistive and resistive force fields [3], [6], [9], [10]. To our knowledge, no other group has studied adaptation of the wrist in 2 DOFs using lateral force fields. Therefore, we aim to determine if existing models of dynamic adaptation appropriately characterize behavior of the wrist. We have chosen three candidate models. The first is a single state model, that is the simplest model capable of describing salient features of adaptation.

$$e(n) = f(n) - x(n) \quad (2)$$

$$x(n+1) = Ax(n) + Be(n) \quad (3)$$

In this model, performance error $e(n)$ is modeled as the difference between the applied force field $f(n)$ and the subject's motor output $x(n)$ (eq. 2). Here, $x(n)$ represents the internal model on trial n , that is combined with performance error $e(n)$ to determine control of the next movement $x(n+1)$ (eq. 3). A is a constant that represents the retention of the previous state (i.e. how much the current state contributes to the next state), while B represents sensitivity to error (i.e. how much performance error will update the next state). Both model parameters are constrained between (0, 1).

The second model is a two-state model proposed by Smith et al [6].

$$x(n) = x_f(n) + x_s(n) \quad (4)$$

$$x_f(n+1) = A_f x_f(n) + B_f e(n) \quad (5)$$

$$x_s(n+1) = A_s x_s(n) + B_s e(n) \quad (6)$$

In this model, (eq. 2) is complemented with eqs. (4-6). The internal model state $x(n)$ is the sum of two states (eq. 4), a fast learning state x_f and a slow learning state x_s . The fast (eq. 5) and slow (eq. 6) states are updated on every trial by performance error $e(n)$ in proportion to their retention (A_f , and A_s) and update parameters (B_f and B_s). For these parameters, $A_f < A_s$ and $B_f > B_s$, as the slow state retains more from trial to trial and is less sensitive to error than the fast state. All parameters are constrained between (0, 1).

The third model we tested is a context-dependent multi-state model proposed by Lee et al [7].

$$x_s(n+1) = A_s x_s(n) + B_s e(n) \cdot c(n) \quad (7)$$

In this model, (eq. 6) of the two-state model is substituted with equation 7. Here, the slow learning state is context dependent and has N inner states equal to the number of dynamic conditions included in the task. Each inner slow state is updated by performance error $e(n)$ only in its corresponding task condition, and is engaged by the contextual cue, $c(n)$ (eq. 7). For our task, there are $N = 2$ inner states, corresponding the clockwise and counter-clockwise force fields (Fig. 2). We assume that slow states are switched by $c(n)$ after error experienced in the first trial of a given perturbation condition. Parameters are related as $A_f < A_s$ and $B_f > B_s$ and constrained between (0,1).

E. Behavioral Analysis

In force field adaptation, the internal model, $x(n)$, can be estimated from two measurements: Trajectory error (TE) measured on non-EC trials, or adaptation index (AI) measured on EC trials spread intermittently throughout the task.

TE was taken as the maximal perpendicular deviation from the straight line connecting the start and end targets in the first 150 ms after velocity onset (Fig. 3), normalized by initial TE measured in the first perturbation trial ($n=101$). Velocity onset was defined as the first instant that goal-directed velocity exceeded 10% of the subject's median maximum velocity across all trials. In this way, TE is measured with limited interference from online error correction processes and most directly reflects the feed-forward commands based on the current state of the internal model [17].

AI is measured during error clamp trials, in which lateral trajectory errors are 'clamped' to 0 such that $x(n) = f(n)$ (eq. 2). In this condition, the robot measures the lateral force profile produced by the subject $f(n)$, which reflects the subject's expectation of required task dynamics. To produce a normalized measure of $x(n)$, AI was determined by regression of the measured force profile onto the ideal force profile necessary to counteract the perturbation, from velocity onset to 150 ms after (Fig. 3) [6], [17]. In this way AI estimation of the internal model is free from online error corrections. Because subjects can reduce trajectory errors due to muscle stiffening and not internal model formation, all measures of adaptation were based on our measures of AI.

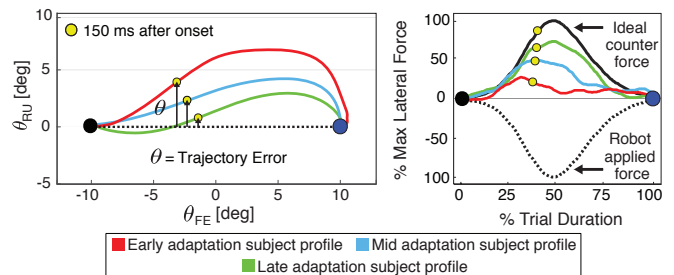


Fig. 3. Behavioral measures of adaptation. On the left is trajectory error, on the right is adaptation index.

To test for *spontaneous recovery*, we took the mean AI measured for each subject in the EC block of the A-B-EC task, and used a Wilcoxon signed rank test to determine if the median AI measured across subjects was significantly different from zero. To test for the presence of *interference* or *dual adaptation* we performed two tests. In the first test, we used a Kruskal-Wallis test to compare the mean AI measured for each subject in the last 8 CW trials of the first alternating force field block (trials 349-356) to the mean AI measured in the last 8 CW trials of the last alternating force field block (trials 541-548). A decrease in AI would indicate retrograde interference, in which learning of the CC force field reduces retention of the CW force field, while an increase in AI would indicate dual adaptation. In the second test, we used a Kruskal-Wallis test to compare AI achieved after exposure to 160 trials of each force field, comparing the mean AI measured in CW trials 253-260 with the mean AI measured in CC trials 573-580 for each subject. CW AI greater than CC would be indicative of anterograde interference, in which prior learning of the CW force field reduces learning of the CC, while no difference would be indicative of dual adaptation.

F. Model Fitting

We used group data for model fitting, calculated as the average AI measured across all subjects, excluding trials with inappropriate trial duration or reversals in goal-directed trajectories ($<2\%$ of trials). For each candidate model, model parameters were estimated by fitting group averaged AI data across the whole task. We also performed a cross-validation analysis to determine how well model parameters estimated from data measured in parts 1 and 2 explained behavior measured in part 3 of the task.

We used the MATLAB `fmincon` function to estimate the parameters A and B (single-state) and A_f , A_s , B_f , and B_s (two-state and multi-state) that minimized the mean squared error between the measured average AI and model predictions of $x(n)$. To prevent our results from being subject to local minima, we seeded `fmincon` with 500 unique initial parameter combinations generated from parameter distributions reported in the literature. The range of initial parameters used were as follows: $\mu_{A/A_f} = \mu = 0.7518$, $[0.1289, 0.9973]$; $\mu_{A_s} = 0.9938$, $[0.9816, 0.9999]$; $\mu_{B/B_f} = 0.2461$, $[0.0067, 0.5757]$; $\mu_{B_s} = 0.1021$, $[0.0022, 0.4129]$. From these 500 parameter estimations, the parameter estimates with the minimum mean squared error were selected.

To evaluate goodness of fit, we calculated the R^2 value between model estimates of TE and AI for each candidate model. To determine if the candidate models captured expected behavioral phenomena, we examined the residuals in specific experimental phases. We defined 9 phases of interest: one for the NF task, three in the A-B-EC task that corresponded to the CW, CC and EC trials, and five in the A-B task that correspond to the 5 repeated CW-CC alternations, denoted as A1-A5 (Fig.2, bottom). We used a Wilcoxon signed rank test to determine if the median residuals in any phase were significantly different from zero, indicative of

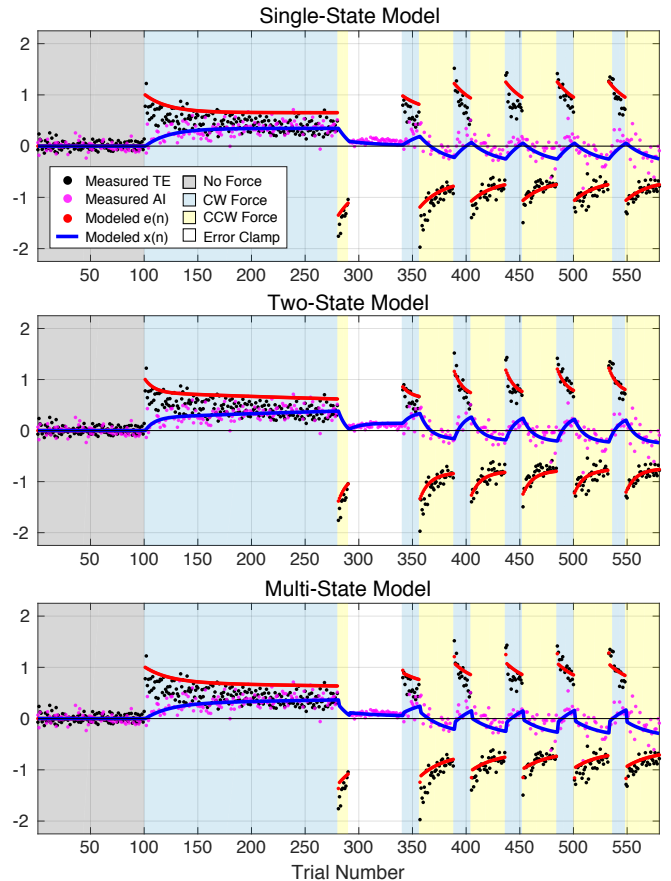


Fig. 4. Model fits to whole task group average AI data.

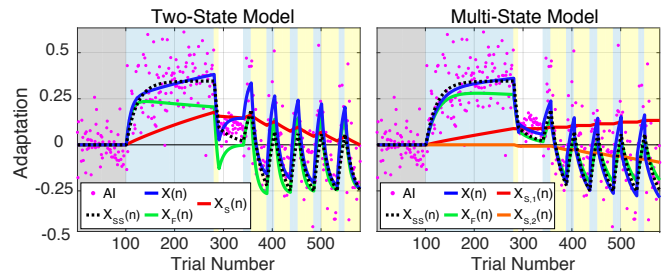


Fig. 5. Evolution and fast and slow states for the Two-state (left) and Multi-state (right) model, given parameter estimates fit to entire task schedule. Single-state evolution is overlaid in black dashed lines for comparison.

model estimation bias. To evaluate model performance in the cross-validation analysis, we used a Kruskal-Wallis test to compare the median squared residuals measured within the 5 unfit blocks (A1-A5) of the alternating A-B task to determine if estimation error was significantly different between candidate models. We used a Bonferonni correction to correct for multiple comparisons, so that significance was set at $p < 0.0021$ for the whole task analysis and $p < 0.0033$ for the cross-validation analysis.

III. RESULTS

A. Behavioral Results

The Wilcoxon signed rank test showed that AI measured in the EC block of the A-B-EC task (median \pm s.e.m.: 0.09

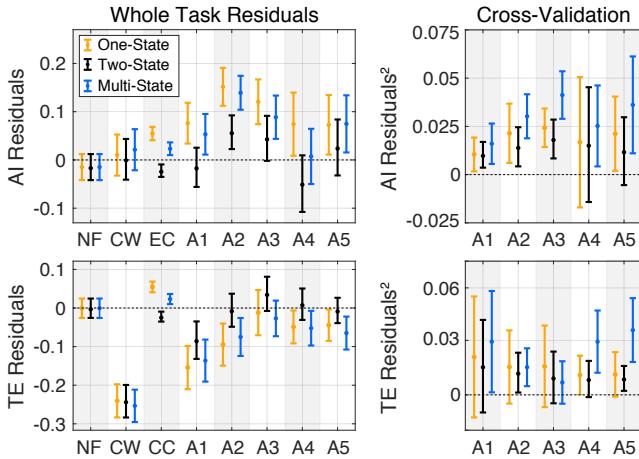


Fig. 6. Left: Median and standard error for residuals fit to whole task data. Biased estimates of AI and TE can be seen predominately in the single state and multi-state models. Right: Median and standard error for squared residuals cross-validation analysis. Error in the A4-A5 blocks is significantly greater for the multi-state model than the other two models

± 0.02) was significantly greater than zero ($p < 0.001$), consistent with spontaneous recovery, as positive AI reflects savings of the initial adaptation to the CW force field. In the alternating force field task, AI measured in trials 349-356 of the first CW block was significantly greater than AI measured in trials 541-548 of the final CW block (0.18 ± 0.05 and 0.06 ± 0.03 respectively, $p = 0.039$), consistent with retrograde interference. The magnitude of AI measured in CW trials 253-260 of the A-B-EC task was significantly greater than AI measured in CC trials 573-580 of the alternating A-B task (0.43 ± 0.05 and -0.20 ± 0.07 respectively, $p = 0.028$), consistent with anterograde interference.

B. Model Comparisons

Model fits to the measured data are shown in Fig. 4. For the whole task, parameter estimates for the single state model were $A = 0.9709$; $B = 0.0154$, and the model fit the combined TE and AI data with an $R^2 = 0.901$. For the two-state model, parameter estimates were $A_f = 0.9194$; $A_s = 0.9987$; $B_f = 0.0265$; $B_s = 0.0016$, with an $R^2 = 0.916$. For the multi-state model, parameter estimates were $A_f = 0.9705$; $A_s = 1.000$; $B_f = 0.0124$; $B_s = 0.0008$, with an $R^2 = 0.898$.

In the cross validation analysis, parameter estimates for the single state model were $A = 0.9768$; $B = 0.0139$, with an $R^2 = 0.904$. For the two-state model, parameter estimates were $A_f = 0.9231$; $A_s = 0.9915$; $B_f = 0.0223$; $B_s = 0.0035$, with an $R^2 = 0.913$. Finally, for the multi-state model parameter estimates were $A_f = 0.9452$; $A_s = 0.9991$; $B_f = 0.0183$; $B_s = 0.0019$ with an $R^2 = 0.879$.

Residuals for each model fit to the whole task are shown in Fig. 6, left. For the single-state model, AI estimation bias in the EC and A2 blocks reached significance, as did TE estimation bias in the CW, CC and A1-A2 blocks. For the two-state model, AI estimation bias in the EC block and TE estimation bias in the CW and A1 blocks reached

significance. For the multi-state model, AI estimation in the EC and A2 blocks and TE estimation in the CW, CC and A1 blocks reached significance.

The squared residuals for our cross validation analysis are shown in Fig. 6, right. Model estimates derived from the first half of the task explained behavior in the second half with a m.s.e. below 0.05 for all models. The two-state model had the smallest error across all task blocks, and the multi-state model had significantly larger error compared to the single and two-state models in blocks A4 and A5 for TE.

IV. DISCUSSION

Our analysis of AI in the alternating A-B task provided evidence for interference, but not for dual adaptation. The significant decrease in CW AI measured over the alternating A-B task is consistent with retrograde interference, in that learning of the CC force field reduced retention of adaptation to the CW force field [6]. The significantly smaller magnitude of CC AI compared to CW AI measured after the same number of trials is consistent with anterograde interference, in that learning of the CW force field reduced learning of the CC force field. Neither result is consistent with dual adaptation, in which AI to both CW and CC force fields should remain the same or increase with additional training.

Analysis of AI in our A-B-EC task showed significant spontaneous recovery that is consistent with results reported in the reaching literature. While our single state model was able to capture the presence of after effects in the error clamp block, the model predicts a decay in AI across the EC block rather than the increase in AI seen over the course of the EC block (Fig. 4 and 5). This misestimation resulted in significant bias in AI residuals fit in the EC block in the single-state model that a post-hoc Kruskal-Wallis test showed was significantly greater than the other two candidate models (Fig. 6, top left).

The multi-state model had the worst R^2 fit in both analyses and the greatest change in parameter estimates between analyses. In the model fit to the whole task, the estimated slow state parameters were $A_s = 1.000$; $B_s = 0.0008$. Because each learning state starts at 0, these parameters result in almost negligible contribution of the slow state, eliminating any benefit of context dependent slow states in describing the adaptive behavior. In fact, comparison between the single-state and the multi-state model can be seen to be roughly equivalent in Fig. 5, right. In the cross-validation analysis, the slow state parameters became $A_s = 0.9413$; $B_s = 0.0024$. The resulting increase in contribution of the context dependent slow states decreased the overall model fit in the alternating task schedule, seen both by the decrease in R^2 and significantly greater squared residual error. These results suggest that the multi-state model is less robust to describing adaptive behavior of the wrist under multiple task schedules, and particularly struggles to model the interference observed in the alternating A-B task.

The model with the highest R^2 value in both the whole task estimation and in the cross validation experiment was the two-state model. Moreover, this model had the least

estimation biases for both the AI and TE estimates. The adaptive behavior of the wrist characterized by this model differs from behavior of the whole arm and elbow in a few important ways. The two-state model fit to our data suggests that adaptation of the wrist is dominated by the fast learning state, with less contribution from the slow learning state than has previously been reported [6], [7]. Typically, by the end of 100 trials, the internal model is dominated by the slow state while the fast state decreases towards zero. Instead, in our task the two states can be seen to be roughly equivalent by the end of 180 trials (Fig. 5, left). Additionally, the end magnitude of adaptation seen in the wrist is less than that observed in reaching. Although subjects performed 180 trials in the CW force field in the A-B-EC task, the average peak adaptation index was just 0.40. In other adaptation tasks, adaptation index is reported as reaching between 0.5-0.7 after just 125 trials [6], [7], [9], [10].

Finally, all models (fit only to adaptation index) predicted larger trajectory errors than were actually measured. This may be due to the control strategy implemented by the CNS to counteract the perturbations. While it is theoretically possible for the CNS to counteract perturbations using purely a feed-forward internal model, it is also possible to reject perturbations through joint stiffening using an impedance control strategy. The CNS has been shown to increase joint stiffness in response to unstable force fields in wrist pointing [3], [17]. While the force fields used in this study were learnable, it is possible such learning is not worth the effort for the low amplitude movements of our task when joint stiffening rejects perturbations to a "tolerable" magnitude.

Whether the results measured here reflect the true characteristic of the wrist or are specific to our robotic exoskeleton remains to be proven. In order to achieve MR-compatibility, certain design constraints have increased the compliance of our robot and reduced its ability to produce perfect error clamp conditions. In future work, we plan to perform the same tasks using a higher powered, less compliant wrist robot, the UDiffWrist [18], to confirm that differences in adaptive behavior of the wrist are not unduly influenced by measurement limitations in our MR-compatible system.

V. CONCLUSION

In our study, we collected data from thirteen subjects performing a wrist pointing task using our wrist robot, the MR-SoftWrist, to characterize adaptation of the wrist to lateral force perturbations. Our task included an A-B-EC force field schedule that elicited spontaneous recovery, and an alternating A-B force field schedule that showed evidence of interference between the two oppositely directed force fields. A two-state model of adaptation best fit behavioral data across both task schedules, and showed that the adaptation process is largely dominated by the fast learning state with lesser engagement of the slow-learning state. Behavioral data provide evidence that the CNS uses internal models to control wrist movements under lateral perturbations, in conjunction with other perturbation rejection strategies.

VI. ACKNOWLEDGMENTS

We acknowledge support from the American Heart Association Scientist Development Grant no.17SDG3369000.

REFERENCES

- [1] H. Rodgers, H. Bosomworth, H. I. Krebs, F. van Wijck, D. Howel, N. Wilson, L. Aird, N. Alvarado, S. Andole, D. L. Cohen, J. Dawson, C. Fernandez-Garcia, T. Finch, G. A. Ford, R. Francis, S. Hogg, N. Hughes, C. I. Price, L. Ternent, D. L. Turner, L. Vale, S. Wilkes, and L. Shaw, "Robot assisted training for the upper limb after stroke (RATULS): a multicentre randomised controlled trial," *The Lancet*, vol. 394, no. 10192, pp. 51–62, 2019.
- [2] R. Shadmehr, "Learning to Predict and Control the Physics of Our Movements," *The Journal of Neuroscience*, vol. 37, no. 7, pp. 1663–1671, 2017.
- [3] R. A. Scheidt, J. L. Zimelman, N. M. Salowitz, A. J. Suminski, K. M. Mosier, J. Houk, and L. Simo, "Remembering forward: Neural correlates of memory and prediction in human motor adaptation," *NeuroImage*, vol. 59, no. 1, pp. 582–600, 2012.
- [4] A. J. Farrens, A. Zonnino, A. Erwin, M. K. O'Malley, C. L. Johnson, D. Ress, and F. Sergi, "Quantitative Testing of fMRI-compatibility of an Electrically Active Mechatronic Device for Robot-Assisted Sensorimotor Protocols," *IEEE Transactions on Biomedical Engineering*, pp. 1–13, 2017.
- [5] A. Erwin, M. K. O'Malley, D. Ress, and F. Sergi, "Kinesthetic Feedback during 2DOF Wrist Movements via a Novel MR-Compatible Robot," *IEEE Transactions on Neural Systems and Rehabilitation Engineering*, vol. 25, no. 9, pp. 1489–1499, 2017.
- [6] M. A. Smith, A. Ghazizadeh, and R. Shadmehr, "Interacting adaptive processes with different timescales underlie short-term motor learning," *PLoS Biology*, vol. 4, no. 6, pp. 1035–1043, 2006.
- [7] J.-Y. Lee and N. Schweighofer, "Dual adaptation supports a parallel architecture of motor memory," *J Neurosci*, vol. 29, no. 33, pp. 10396–10404, 2009.
- [8] R. Osu, D. W. Franklin, H. Kato, H. Gomi, K. Domen, T. Yoshioka, and M. Kawato, "Short- and long-term changes in joint co-contraction associated with motor learning as revealed from surface EMG," *Journal of Neurophysiology*, vol. 88, no. 2, pp. 991–1004, 2002.
- [9] S. E. Criscimagna-Hemminger and R. Shadmehr, "Consolidation patterns of human motor memory," *Journal of Neuroscience*, vol. 28, no. 39, pp. 9610–9618, 2008.
- [10] G. C. Sing and M. A. Smith, "Reduction in learning rates associated with anterograde interference results from interactions between different timescales in motor adaptation," *PLoS Computational Biology*, vol. 6, no. 8, 2010.
- [11] H. Imamizu, N. Sugimoto, R. Osu, K. Tsutsui, K. Sugiyama, Y. Wada, and M. Kawato, "Explicit contextual information selectively contributes to predictive switching of internal models," *Experimental Brain Research*, vol. 181, no. 3, pp. 395–408, 2007.
- [12] H. Imamizu and M. Kawato, "Neural correlates of predictive and postdictive switching mechanisms for internal models," *Journal of Neuroscience*, vol. 28, no. 42, pp. 10751–10765, 2008.
- [13] A. J. Suminski, S. M. Rao, K. M. Mosier, and R. A. Scheidt, "Neural and electromyographic correlates of wrist posture control," *Journal of Neurophysiology*, vol. 97, no. 2, pp. 1527–1545, 2007.
- [14] S. K. Charles and N. Hogan, "Dynamics of wrist rotations," *Journal of Biomechanics*, vol. 44, no. 4, pp. 614–621, 2011.
- [15] R. C. Miall, N. Jenkinson, and K. Kulkarni, "Adaptation to rotated visual feedback: A re-examination of motor interference," *Experimental Brain Research*, vol. 154, no. 2, pp. 201–210, 2004.
- [16] A. J. Farrens, A. Zonnino, and F. Sergi, "Effects of force-field adaptation on neural activation and resting-state functional connectivity," *International Conference on NeuroRehabilitation*, pp. 1–2, 2018.
- [17] T. E. Milner, "Adaptation to destabilizing dynamics by means of muscle cocontraction," *Experimental Brain Research*, vol. 143, no. 4, pp. 406–416, 2002.
- [18] A. Zonnino and F. Sergi, "Optimal design of cable differential actuation for 2-DOF wrist robots : effect of joint misalignments on interaction force," *Engineering in Medicine and Biology Conference* 2, 2016.